

Relativistic many-body calculations of dielectronic satellite spectra created by autoionizing $1s2l2l'$ states in Li-like ions

U I Safronova¹, A S Safronova¹ and W R Johnson²

¹ Physics Department, University of Nevada, Reno, NV 89557, USA

² Department of Physics, 225 Nieuwland Science Hall, University of Notre Dame, Notre Dame, IN 46556, USA

E-mail: ulyanas@unr.edu, alla@unr.edu and johnson@nd.edu

Received 2 September 2009, in final form 13 December 2009

Published DD MMM 2010

Online at stacks.iop.org/JPhysB/43/000000

Abstract

Relativistic many-body perturbation theory (RMBPT), including the Breit interaction, is used to evaluate energy levels, radiative matrix elements and autoionization rates for $1s2l2l'$ states of lithium-like Mo^{39+} , Pr^{56+} , W^{71+} and Hg^{77+} . Radiative and non-radiative data are combined to obtain branching ratios, intensities and effective emission rate coefficients of dielectronic satellite lines. Relative intensity factors are shown graphically for the $1s2l'2l''-1s^22l$ radiative transitions in lithium-like ions with nuclear charges Z ranging from 6 to 100; however, our emphasis here is on dielectronic recombination rates in the four lithium-like ions listed above. Such data, for high- Z ions in particular, are relevant to spectroscopic diagnostics of very high-temperature plasmas including future experiments at the International Thermonuclear Experimental Reactor.

(Some figures in this article are in colour only in the electronic version)

1. Introduction

High- Z materials such as tungsten will be used in plasma-facing components for future experiments at the International Thermonuclear Experimental Reactor (ITER). The effect of sputtered impurities on ITER plasmas, in particular from heavy ions, should be controlled to limit radiation losses. Tungsten plasmas might reach the reactor core and hence attain temperatures of 20–40 keV and might be ionized to Li-like ions. Spectroscopy will be used to monitor the impurity influx. Therefore, creation of an atomic database for highly ionized ions is of great importance (see [1–3]). For example, spectroscopy of highly charged tungsten ions relevant to fusion plasmas was recently discussed by Biedermann *et al* [2] who emphasized the need for spectroscopic information on radiation from tungsten ions. The need for such data is driven by the use of tungsten as the plasma-facing material in present-day experimental fusion devices, such as the Axially Symmetric Divertor Experiment (ASDEX Upgrade), the Joint European Torus (JET) and ITER. Work on tungsten from various laboratories and recent results for

highly ionized W from the Electron Beam Ion Trap (EBIT) at the National Institute of Standards and Technology (NIST) were discussed by Reader in [3]. Loch *et al* [4] reported their efforts aimed at improving the atomic data that was used in modelling tungsten spectral emission from tokamak plasmas in [4].

The importance of dielectronic satellite spectra of Li-like ions as a plasma diagnostic has been recognized for almost 40 years [5]. In particular, dielectronic satellites (DS) created by $1s2lnl'$ autoionizing states have been extensively studied both theoretically [5–20] and experimentally [21–28] both in astrophysical and laboratory plasmas including tokamak plasmas. However, properties of ions with nuclear charge Z greater than 54 have been considered in only a few publications. These papers primarily discuss experiments performed with EBIT devices. Indeed, EBITs play an important role in obtaining experimental data used to benchmark theoretical calculations for various applications, including magnetic fusion diagnostics [29]. Recently, measurements of the K -shell spectrum of He-like through Be-like praseodymium ions were made with the

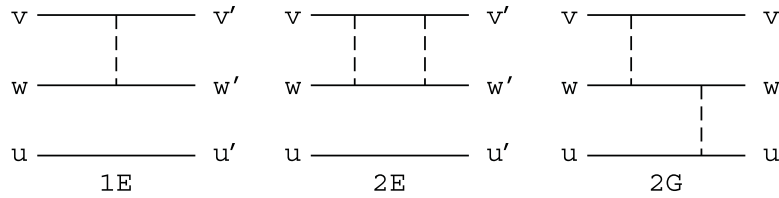


Figure 1. Brueckner–Goldstone diagrams for first-order (1E) and second-order (2E and 2G) contributions to the energy matrix for three-electron ions. The dashed lines designate Coulomb + Breit interactions and solid lines designate electrons in different states.

Livermore SuperEBIT [30]. The measured transition energies $(1s2s2p_{3/2})_{3/2} \rightarrow (1s^22s)_{1/2}$ and $(1s2s^2)_{1/2} \rightarrow (1s^22p_{3/2})_{1/2}$ were compared with theoretical calculations from several atomic codes [30]. Photorecombination of highly charged few-electron mercury ions (Hg^{75+} – Hg^{78+}) was explored with the Heidelberg EBIT [31, 32]. Evidence for strong Breit interaction in dielectronic recombination of highly charged heavy ions was obtained by Nobuyuki Nakamura *et al* [33] who measured resonance strengths for dielectronic recombination of Li-like iodine, holmium and bismuth using an EBIT.

In the present paper, relativistic many-body perturbation theory (RMBPT) is used to determine branching ratios, intensity factors and effective emission rate coefficients of $1s2l2l' - 1s^22l''$ dielectronic satellite lines in lithium-like ions. To determine those properties, we calculated transition energies, radiative transition rates for all spin-allowed and spin-forbidden electric dipole transitions, and non-radiative transition rates for the autoionizing $1s2l2l'$ states.

The difference between our RMBPT code and the multi-configuration Dirac–Fock (MCDF) code used in [12, 13, 18, 19] is in additional second-order contributions that are not included in the MCDF approximation. The difference between our RMBPT method and the non-relativistic many-body perturbation theory method used in [6, 8, 10, 15–17, 20] is similar to the difference between MCDF and MCHF approaches.

Several recent publications concerning $1s2l2l'$ autoionizing states provide additional motivation for the present research. Wavelengths, radiative transition probabilities, oscillator strengths and line strengths for the $1s2s2p - 1s^22s$ lines in Mo^{39+} and Fe^{23+} were calculated using the MCDF approach in [18, 19]. The contribution of radiative cascades from all high- n states to intensities of the $1s2l2l' - 1s^22l''$ satellites for ions from Ne^{7+} to Zn^{27+} was investigated in [20].

In the present paper, we give a detailed discussion of the factors (energies, radiative transition rates and autoionization rates) that enter calculations of dielectronic recombination rates for lithium-like ions. We discuss these factors in detail for the important case of lithium-like tungsten. Synthetic spectra of dielectronic satellite lines ($1s2l2l' - 1s^22l''$) from the Mo^{39+} and W^{71+} ions are evaluated using our RMBPT data. Trends of intensity factors as functions of nuclear charge Z are shown graphically. We test the accuracy of our calculations by comparing our results with precise measurements.

2. Energy levels, transition probabilities and autoionization rates

Detailed calculations of dielectronic recombination (DR) parameters require energies, radiative transition probabilities and autoionization rates for atomic states in the recombined ion. In the paragraphs below, we present values for these quantities, together with a brief discussion of how they are obtained, for the $1s2l2l'$ states.

2.1. Energy levels

The present calculations of energies are carried out using single-particle orbitals calculated in the unscreened nuclear Coulomb potential including finite nuclear size. A detailed explanation of how the energies of three-particle states are obtained within the RMBPT framework is given in [34]. Briefly, we calculate the first- and second-order two-particle matrix elements for He-like ions, and recouple them as described in [34], to obtain the contributions from all diagrams of the type shown in figure 1 (1E and 2E). These matrix elements are combined to obtain the two-particle contributions to energies of Li-like ions. Intrinsically, three-particle diagrams of the type shown in figure 1 (2G) also contribute to the second-order energy for Li-like ions. A detailed discussion of various contributions for Fe^{23+} was given in [34]. We skip some details mentioned in [34] and summarize our results for Li-like tungsten, W^{71+} .

In table 1, we list the following contributions to the energies of the 16 possible doubly excited $1s2l2l'$ states in W^{71+} . The notation is as follows: $E^{(n)}$ designates the n th order Coulomb energy, $B^{(n)}$ designates the n th order Coulomb–Breit energy and $E^{(0+1)} = E^{(0)} + E^{(1)} + B^{(1)}$. The QED correction is designated by E_{LAMB} and the total theoretical energy relative to the $1s$ state is designated by E_{tot} .

The present approach was used to evaluate energies of Be-like, B-like and Zn-like ions in [35–37]. Both jj and LS designations are given in table 1; however, neither jj - nor LS -coupling describes the *physical* states properly, except for the single-configuration state $2s_{1/2}2p_{3/2}(2)1s [5/2] \equiv 2s2p(^3P)1s^4P_{5/2}$. We find that the second-order energy is the dominant contribution among the other corrections to $E^{(0+1)}$ for $1s2p^2$ states. However, E_{LAMB} increases rapidly with Z and is larger than the second-order contribution for the $1s2s2p$ and $1s2s^2$ states in Li-like tungsten.

The Lamb contributions can be determined approximately using the one-electron hydrogenic Lamb shift data given in

Table 1. Contributions to the energy levels of Li-like tungsten, $Z = 74$ in au, $E^{(0+1)} = E^{(0)} + E^{(1)} + B^{(1)}$.

LS -coupling	$E^{(0+1)}$	$E^{(2)}$	$B^{(2)}$	E_{LAMB}	E_{tot}	jj -coupling
$2s2p(^3P)1s^4P_{1/2}$	-1467.2396	-0.3697	-0.0739	0.8478	-1466.8354	$2s_{1/2}2p_{1/2}(0)1s$
$2s2p(^3P)1s^2P_{1/2}$	-1461.3756	-0.5452	-0.0919	0.8478	-1461.1649	$2s_{1/2}2p_{1/2}(1)1s$
$2s2p(^1P)1s^2P_{1/2}$	-1406.3812	-0.4318	-0.0335	0.9182	-1405.9282	$2s_{1/2}2p_{3/2}(1)1s$
$2s2p(^3P)1s^4P_{3/2}$	-1467.3233	-0.4131	-0.0051	0.8479	-1466.8935	$2s_{1/2}2p_{1/2}(1)1s$
$2s2p(^3P)1s^2P_{3/2}$	-1408.4333	-0.3875	-0.0261	0.9182	-1407.9287	$2s_{1/2}2p_{3/2}(1)1s$
$2s2p(^1P)1s^2P_{3/2}$	-1403.9707	-0.4741	-0.0689	0.9183	-1403.5954	$2s_{1/2}2p_{3/2}(2)1s$
$2s2p(^1P)1s^4P_{5/2}$	-1411.8007	-0.2939	-0.0050	0.9183	-1411.1813	$2s_{1/2}2p_{3/2}(2)1s$
$2s^2(^1S)1s^2S_{1/2}$	-1470.1595	-0.3391	-0.0366	1.5166	-1469.0187	$2s_{1/2}2s_{1/2}(0)1s$
$2p^2(^3P)1s^4P_{1/2}$	-1458.0132	-0.5913	-0.0817	0.1781	-1458.5081	$2p_{1/2}2p_{1/2}(0)1s$
$2p^2(^3P)1s^2P_{1/2}$	-1401.8039	-0.5389	-0.0437	0.1877	-1402.1988	$2p_{3/2}2p_{3/2}(0)1s$
$2p^2(^1S)1s^2S_{1/2}$	-1342.4158	-0.4979	-0.0613	0.2592	-1342.7159	$2p_{1/2}2p_{3/2}(1)1s$
$2p^2(^3P)1s^4P_{3/2}$	-1402.7388	-0.4373	-0.0836	0.1878	-1403.0720	$2p_{1/2}2p_{3/2}(1)1s$
$2p^2(^1D)1s^2D_{3/2}$	-1400.7072	-0.5637	-0.0587	0.1878	-1401.1418	$2p_{1/2}2p_{3/2}(2)1s$
$2p^2(^3P)1s^2P_{3/2}$	-1343.5532	-0.4912	-0.0461	0.2583	-1343.8323	$2p_{3/2}2p_{3/2}(2)1s$
$2p^2(^3P)1s^4P_{5/2}$	-1403.1568	-0.5002	-0.0058	0.1878	-1403.4750	$2p_{1/2}2p_{3/2}(2)1s$
$2p^2(^3P)1s^2D_{5/2}$	-1346.0605	-0.3999	-0.0208	0.2582	-1346.2230	$2p_{3/2}2p_{3/2}(2)1s$

Table 2. QED corrections (eV) for Li-like ions. Present results (a) given by a phenomenological approach (see the text) are compared with *ab initio* results of (b) Blundell [42], (c) Yerokhin *et al* [43] and screened QED correction based on approximate methods (d) Y-K Kim *et al* [44].

Z	$2s-2p_{1/2}$			$2s-2p_{3/2}$		
	(a)	(b, c)	(d)	(a)	(b, c)	(d)
10	-0.0135	-0.0141 ^b	-0.0144	-0.0131	-0.0135 ^b	-0.0139
12	-0.0281	-0.0282 ^b	-0.0291	-0.0265	-0.0269 ^b	-0.0279
15	-0.0654	-0.066 ^b	-0.0674	-0.0615	-0.062 ^b	-0.0641
18	-0.129	-0.130 ^b	-0.132	-0.120	-0.122 ^b	-0.125
20	-0.187	-0.191 ^b	-0.193	-0.174	-0.178 ^b	-0.182
30	-0.809	-0.810 ^b	-0.819	-0.741	-0.743 ^b	-0.755
32	-1.016	-1.016 ^b	-1.026	-0.933	-0.929 ^b	-0.943
40	-2.222	-2.22 ^b	-2.231	-2.028	-2.00 ^b	-2.028
42	-2.629	-2.63 ^b	-2.642	-2.396	-2.37 ^b	-2.397
50	-4.857	-4.81 ^b	-4.832	-4.410	-4.31 ^b	-4.352
54	-6.372	-6.29 ^b	-6.308	-5.778	-5.62 ^b	-5.669
60	-9.268	-9.08 ^b	-9.097	-8.392	-8.11 ^b	-8.165
70	-16.20	-15.61 ^b	-15.61	-14.64	-13.99 ^b	-14.06
74	-19.88		-19.00	-17.96		-17.19
80	-26.62	-25.12 ^b	-25.09	-24.02	-22.82 ^b	-22.93
83	-30.60		-28.64	-27.60	-26.28 ^c	-26.35
90	-41.76	-38.45 ^b	-38.36	-37.56	-35.87 ^b	-36.02
92	-45.48	-41.68 ^b	-41.57	-40.88		-39.32
92		-41.55 ^c				

[38–41] with $Z \rightarrow Z - 1$ for $2lj$ states (in the case of the $1s^22lj$ state in Li-like neon, for example, we use the $2lj$ hydrogenic Lamb shift data obtained for $Z = 9$). In table 2, we compare our one-electron QED corrections for the $1s^22s-1s^22p_j$ transitions in Li-like ions with the *ab initio* results of Blundell [42], Yerokhin *et al* [43] and screened QED correction based on approximate methods of Y-K Kim *et al* [44]. We see that the disagreement between our phenomenological values for one-electron QED and results from [42] is about 3–5% for ions with $Z = 10-70$ and about 5–10% for ions with $Z = 80-92$. It should be noted that our values are in better agreement with the *ab initio* results of [42] than with the screened results of Y-K Kim *et al* [44].

2.2. Dipole matrix elements

Details of the RMBPT method for calculation of the E1 radiative transition rates in three-particle systems were given in [45]. In this section, we discuss reduced E1 matrix elements between doubly excited and singly excited states in Li-like ions. In particular, we calculate the first- and second-order two-particle matrix elements for He-like ions, and recouple them as described in [45], to obtain the contributions from the first- and second-order diagrams shown in figure 2. It should be noted that in comparison with boron-like systems [45], there is only one correlation diagram for the second-order matrix elements since we consider Li-like systems as systems with three electrons and an empty core.

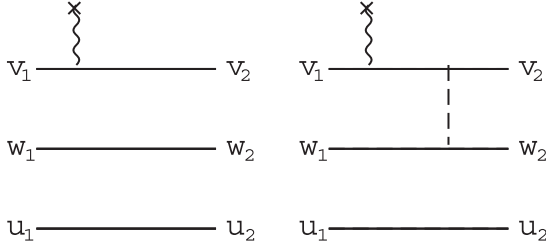


Figure 2. First- and second-order Brueckner–Goldstone diagrams for dipole matrix elements in the three-electron system.

Table 3. Coupled reduced matrix elements $2I2I'(^{1,3}L_{12})1s^{2,4}L_J-1s^22I^2L'_J$, calculated in length and velocity forms for W^{71} . Velocity-form matrix elements are given (a) with and (b) without negative-energy contributions.

$2I2I'(^{1,3}L)1s$	length	velocity ^a	velocity ^b
$2s^2p(^{1,3}P)1s^{2,4}P_J-1s^2s^2S_{1/2}$ transition			
$2s2p(^3P)1s^4P_{1/2}$	0.006 736	0.006 736	0.006 748
$2s2p(^3P)1s^2P_{1/2}$	0.008 304	0.008 304	0.008 318
$2s2p(^1P)1s^2P_{1/2}$	0.013 422	0.013 422	0.013 446
$2s2p(^3P)1s^4P_{3/2}$	0.014 531	0.014 531	0.014 559
$2s2p(^3P)1s^2P_{3/2}$	0.017 350	0.017 349	0.017 382
$2s2p(^1P)1s^2P_{3/2}$	0.008 781	0.008 781	0.008 797
$2I^2(^{1,3}L)1s^{2,4}L_J-1s^22p^2P_{1/2}$ transition			
$2s^2(^1S)1s^2S_{1/2}$	0.002 504	0.002 504	0.002 510
$2p^2(^3P)1s^4P_{1/2}$	0.012 482	0.012 482	0.012 506
$2p^2(^3P)1s^2P_{1/2}$	0.013 711	0.013 711	0.013 736
$2p^2(^1S)1s^2S_{1/2}$	0.000 089	0.000 089	0.000 091
$2p^2(^3P)1s^4P_{3/2}$	0.006 312	0.006 312	0.006 326
$2p^2(^1D)1s^2D_{3/2}$	0.017 429	0.017 428	0.017 465
$2p^2(^3P)1s^2P_{3/2}$	0.000 076	0.000 076	0.000 077
$2I^2(^{1,3}L)1s^{2,4}L_J-1s^22p^2P_{3/2}$ transition			
$2s^2(^1S)1s^2S_{1/2}$	0.000 309	0.000 308	0.000 310
$2p^2(^3P)1s^4P_{1/2}$	0.000 158	0.000 158	0.000 158
$2p^2(^3P)1s^2P_{1/2}$	0.010 461	0.010 461	0.010 479
$2p^2(^1S)1s^2S_{1/2}$	0.011 774	0.011 774	0.011 796
$2p^2(^3P)1s^4P_{3/2}$	0.012 464	0.012 464	0.012 486
$2p^2(^1D)1s^2D_{3/2}$	0.008 314	0.008 314	0.008 327
$2p^2(^3P)1s^2P_{3/2}$	0.023 513	0.023 512	0.023 553
$2p^2(^3P)1s^4P_{5/2}$	0.018 049	0.018 049	0.018 087
$2p^2(^3P)1s^2D_{5/2}$	0.012 064	0.012 064	0.012 090

In table 3, we present values of the 22 $2I2I'(^{1,3}L_{12})1s^{2,4}L_J-1s^22I^2L'_J$ coupled reduced matrix elements in the length (L) and velocity (V) forms for Li-like tungsten, $Z = 74$. Although we use an intermediate-coupling scheme, it is nevertheless convenient to label the physical states using the $[LSJ]$ designation. It should be noted that velocity-form matrix elements are given (a) with and (b) without negative-energy contributions.

Negative-energy state (NES) contributions to the second-order reduced matrix elements arise from terms in the sums over states for which $\varepsilon < -mc^2$. The NES contributions for non-relativistically allowed transitions were discussed in [46] for He-like ions, where they were found to be important for velocity-form matrix elements; they do not significantly modify length-form matrix elements. In addition, it was shown in [46] that the inclusion of NES is necessary to ensure gauge independence. This is confirmed in table 3; the velocity-form

Table 4. Matrix elements for autoionizing widths $\Gamma(2l_1j_12l_2j_2(J_{12})1s, 2l_3j_32l_4j_4(J_{34})1s)$ (au) in the case of Li-like tungsten, $Z = 74$.

$2l_1j_12l_2j_2(J_{12})1s$	$2l_3j_32l_4j_4(J_{34})1s$	$\Gamma(\text{au})$
Odd-parity states, $J = 1/2$		
$2s_{1/2}2p_{1/2}(0)1s$	$2s_{1/2}2p_{1/2}(0)1s$	8.704[−4]
$2s_{1/2}2p_{1/2}(1)1s$	$2s_{1/2}2p_{1/2}(1)1s$	5.408[−3]
$2s_{1/2}2p_{3/2}(1)1s$	$2s_{1/2}2p_{3/2}(1)1s$	9.275[−4]
$2s_{1/2}2p_{1/2}(0)1s$	$2s_{1/2}2p_{1/2}(1)1s$	2.169[−3]
$2s_{1/2}2p_{1/2}(0)1s$	$2s_{1/2}2p_{3/2}(1)1s$	−8.985[−4]
$2s_{1/2}2p_{1/2}(1)1s$	$2s_{1/2}2p_{3/2}(1)1s$	−2.239[−3]
Even-parity states, $J = 5/2$		
$2p_{1/2}2p_{3/2}(2)1s$	$2p_{1/2}2p_{3/2}(2)1s$	2.611[−3]
$2p_{3/2}2p_{3/2}(2)1s$	$2p_{3/2}2p_{3/2}(2)1s$	1.113[−3]
$2p_{1/2}2p_{3/2}(2)1s$	$2p_{3/2}2p_{3/2}(2)1s$	1.705[−3]

matrix elements given with NES contributions are in complete agreement with length-form matrix elements.

2.3. Autoionization widths of levels as imaginary parts of energy

Autoionizing states differ from other excited states owing to the existence of non-radiative decay channels (e.g. $1s2I2I' \rightarrow 1s^2 + kl''$). The autoionization half-width Γ is the imaginary part of the energy of the autoionizing state as discussed in [47, 48]. The full width (2Γ) is the sum of autoionization transition rates A_a over all channels. For the $n_1^0j_1^0n_2^0j_2^0[J_{12}]1s, J \rightarrow 1s^2kj_n$ transitions, we use the definition given in [49, 50]. Numerical values for the matrix elements $2\Gamma(2l_1j_12l_2j_2(J_{12})1s, 2l_3j_32l_4j_4(J_{34})1s)$ for autoionizing widths in the case of Li-like tungsten, $Z = 74$, are presented in table 4. The resulting matrix elements are coupled in the usual way:

$$\Gamma(Q) = \sum_{Q'} C(Q, Q') \Gamma(Q', Q'') C(Q'', Q), \quad (1)$$

where $C(Q, Q')$ are the intermediate coupling coefficients obtained in the first-order RMBPT. Our final results are given in table 5.

In the second, third and fourth columns of table 5, we list wavelengths λ , radiative rates A_r and sums of radiative rates, respectively, for the $1s2I2I'-1s^22I'$ transitions in W^{71+} . Autoionization rates A_a and Auger energies E_S for the $1s2I2I'$ states are given in columns 5 and 6, respectively. The jj designations used in the previous tables are shown in the last two columns of table 5. In the first column of this table, we present designations used in [8, 20] and many other publications. The states were labelled as follows: $E = 2s^2(^1S)1s$, $C = 2s2p(^1P)1s$, $K = 2s2p(^3P)1s$, $F = 2p^2(^1S)1s$, $F = 2p^2(^1D)1s$, $M = 2p^2(^3P)1s$, $S = 1s^22s$ and $P = 1s^22p$. Digits after a letter (i.e. F212) stand for $(2S+1)(2L+1)(2J+1)$.

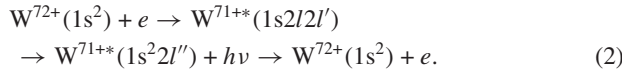
3. Dielectronic satellite spectra

In the dielectronic recombination process for Li-like ions an electron is captured by a He-like ion to an autoionizing state

Table 5. Wavelengths (λ in Å), radiative rates (A_r in s^{-1}), autoionization rates (A_a in s^{-1}), Auger energies (E_S in keV), branching ratio (K), intensity factors (Q_d in s^{-1}) and effective emission rate coefficients (C_S^{eff} in $\text{cm}^3 s^{-1}$) ($T_e = 40$ keV) for the $1s2l'2l''-1s^22l''$ transitions in Li-like tungsten. Designations: $E = 2s^2(^1S)1s$, $C = 2s2p(^1P)1s$, $K = 2s2p(^3P)1s$, $F = 2p^2(^1S)1s$, $F = 2p^2(^1D)1s$, $M = 2p^2(^3P)1s$, $S = 1s^22s$ and $P = 1s^22p$. Digits after a letter (i.e. $F212$) stand for $(2S+1)(2L+1)(2J+1)$. $A[B]$ means $A \times 10^B$.

LS labels	λ	A_r	$\sum A_r$	A_a	E_S	K	Q_d	C_S^{eff}	jj designations	
$F212-P232$	0.1996	1.03[12]	1.63[16]	2.61[13]	42.655	6.31E[-5]	3.29[09]	7.41[-16]	$2p_{1/2}2p_{3/2}(1)1s\ 1/2$	$2p_{1/2}$
$M234-P232$	0.1997	2.14[11]	3.25[16]	3.84[13]	42.624	6.58E[-6]	1.01[09]	2.28[-16]	$2p_{3/2}2p_{3/2}(2)1s\ 3/2$	$2p_{1/2}$
$C234-S212$	0.2044	4.56[15]	4.56[15]	1.09[14]	40.999	9.77E[-1]	4.25[14]	9.98[-11]	$2s_{1/2}2p_{3/2}(2)1s\ 3/2$	$2s_{1/2}$
$F212-P234$	0.2045	1.63[16]	1.63[16]	2.61[13]	42.655	9.98E[-1]	5.20[13]	1.17[-11]	$2p_{1/2}2p_{3/2}(1)1s\ 1/2$	$2p_{3/2}$
$C232-S212$	0.2046	2.12[16]	2.12[16]	4.49[13]	40.936	9.98E[-1]	8.95[13]	2.10[-11]	$2s_{1/2}2p_{3/2}(1)1s\ 1/2$	$2s_{1/2}$
$M234-P234$	0.2046	3.25[16]	3.25[16]	3.84[13]	42.624	9.99E[-1]	1.54[14]	3.47[-11]	$2p_{3/2}2p_{3/2}(2)1s\ 3/2$	$2p_{3/2}$
$K234-S212$	0.2048	1.77[16]	1.77[16]	8.80[13]	40.881	9.95E[-1]	3.50[14]	8.24[-11]	$2s_{1/2}2p_{3/2}(1)1s\ 3/2$	$2s_{1/2}$
$F254-P232$	0.2048	1.90[16]	2.26[16]	1.36[14]	41.065	8.35E[-1]	4.53[14]	1.06[-10]	$2p_{1/2}2p_{3/2}(2)1s\ 3/2$	$2p_{1/2}$
$F256-P234$	0.2049	5.70[15]	5.70[15]	1.05[14]	42.559	9.82E[-1]	6.16[14]	1.39[-10]	$2p_{3/2}2p_{3/2}(2)1s\ 5/2$	$2p_{3/2}$
$M232-P232$	0.2049	2.20[16]	3.39[16]	1.22[12]	41.036	6.49E[-1]	1.58[12]	3.71[-13]	$2p_{3/2}2p_{3/2}(0)1s\ 1/2$	$2p_{1/2}$
$M434-P232$	0.2050	2.49[15]	1.08[16]	9.07[12]	41.012	2.30E[-1]	8.33[12]	1.95[-12]	$2p_{1/2}2p_{3/2}(1)1s\ 3/2$	$2p_{1/2}$
$K232-S212$	0.2098	7.54[15]	7.54[15]	2.54[14]	39.433	9.67E[-1]	4.91[14]	1.20[-10]	$2s_{1/2}2p_{1/2}(1)1s\ 1/2$	$2s_{1/2}$
$F254-P234$	0.2100	3.62[15]	2.26[16]	1.36[14]	41.065	1.59E[-1]	8.63[13]	2.02[-11]	$2p_{1/2}2p_{3/2}(2)1s\ 3/2$	$2p_{3/2}$
$M232-P234$	0.2102	1.19[16]	3.39[16]	1.22[12]	41.036	3.51E[-1]	8.57[11]	2.01[-13]	$2p_{3/2}2p_{3/2}(0)1s\ 1/2$	$2p_{3/2}$
$M434-P234$	0.2102	8.35[15]	1.08[16]	9.07[12]	41.012	7.70E[-1]	2.79[13]	6.55[-12]	$2p_{1/2}2p_{3/2}(1)1s\ 3/2$	$2p_{3/2}$
$M432-P232$	0.2103	1.69[16]	1.69[16]	5.82[12]	39.504	1.00E[0]	1.16[13]	2.83[-12]	$2p_{1/2}2p_{1/2}(0)1s\ 1/2$	$2p_{1/2}$
$M436-P234$	0.2103	1.18[16]	1.18[16]	4.93[13]	41.001	9.96E[-1]	2.95[14]	6.92[-11]	$2p_{1/2}2p_{3/2}(2)1s\ 5/2$	$2p_{3/2}$
$K432-S212$	0.2104	1.14[16]	1.14[16]	1.91[12]	39.278	1.00E[0]	3.83[12]	9.39[-13]	$2s_{1/2}2p_{1/2}(1)1s\ 3/2$	$2s_{1/2}$
$K434-S212$	0.2104	1.14[16]	1.14[16]	1.59[13]	39.277	9.99E[-1]	6.34[13]	1.55[-11]	$2s_{1/2}2p_{1/2}(1)1s\ 3/2$	$2s_{1/2}$
$E212-P232$	0.2113	6.76[14]	6.87[14]	2.42[14]	39.219	7.28E[-1]	3.52[14]	8.64[-11]	$2s_{1/2}2s_{1/2}(0)1s\ 1/2$	$2p_{1/2}$
$M432-P234$	0.2158	2.42[12]	1.69[16]	5.82[12]	39.504	1.43E[-4]	1.67[09]	4.07[-16]	$2p_{1/2}2p_{1/2}(0)1s\ 1/2$	$2p_{3/2}$
$E212-P234$	0.2168	1.05[13]	6.87[14]	2.42[14]	39.219	1.13E[-2]	5.48[12]	1.34[-12]	$2s_{1/2}2s_{1/2}(0)1s\ 1/2$	$2p_{3/2}$

of the resulting Li-like ion followed by radiative decay to a singly-excited bound state:



The ground state of W^{72+} , $1s^2$, is the initial state. The $1s2l'$ states are autoionizing intermediate states. During the DR process, a dielectronic satellite photon, $h\nu$, is emitted when the electron jumps from a doubly excited autoionizing state to a singly excited bound state, $1s^22l'$. Radiative transitions from the doubly excited $1s2l'2l''$ states to the $1s^22l''$ states give rise to satellite lines to the $1s2p-1s^2$ transitions in He-like tungsten.

Branching ratios $K(i, j)$ and relative intensity factors Q_d of the dielectronic satellite (DS) lines are defined as follows (see, for example, [51]):

$$\begin{aligned} K(i, i_0) &= \frac{A_a(i, i_0)}{\sum_{i'_0} A_a(i, i'_0) + \sum_j A_r(i, j)} \\ Q_d(j, i) &= g(i)A_r(j, i)K(j, i) \end{aligned} \quad (3)$$

Here, j denotes the bound state, i is the autoionizing state, i_0 is the initial state (that is, the ground state $1s^2$ of He-like tungsten) and i'_0 is the possible final state for autoionization, which in our case is the same as i_0 . The statistical weight of the initial state i_0 is $g_0 = 1$, $g(i)$ is the statistical weight of the doubly excited state, $A_a(i, i_0)$ is the rate of autoionization from i to i_0 , $A_r(j, i)$ is the radiative rate from i to j .

Assuming a Maxwellian distribution, the effective emission rate coefficient of the dielectronic satellite line is obtained as follows (see, for example, [52]):

$$C_S^{\text{eff}}(j, i) = 3.3 \times 10^{-24} \left(\frac{I_H}{kT_e} \right)^{3/2} \frac{Q_d(j, i)}{g_0}$$

$$\times \exp\left(-\frac{E_S(i)}{kT_e}\right) \text{photons cm}^3 \text{s}^{-1}, \quad (4)$$

where I_H is the ionization potential of hydrogen, $E_S(i)$ is the energy of the autoionizing state i relative to $1s^2$ and T_e is the electron temperature.

As mentioned above, the sum of autoionization rates ($\sum_{i'_0} A_a(i, i'_0)$) includes only one term, $i'_0 = i_0$. The values of $A_a(i, i_0)$ (below, we omit the index i_0) and $E_S(i)$ for the 22 transitions are presented in columns 5 and 6 of table 5, respectively. The wavelengths λ , radiative rates $A_r(j, i)$ and sums of radiative rates $\sum_k A_r(k, i)$ for electric-dipole transitions are given in columns 2, 3 and 4 of table 5, respectively. Columns 7, 8 and 9 list branching ratios K , relative intensity factors $Q_d(j, i)$ and effective emission rate coefficients $C_S^{\text{eff}}(j, i)$, respectively, defined by equation (4). Values of $C_S^{\text{eff}}(j, i)$ are given for $T_e = 40$ keV.

Most of the transitions listed in table 5 are one-electron $2p_{1/2}-1s$ and $2p_{3/2}-1s$ transitions. For those transitions, the branching ratio K is almost equal to 1 (lines 3–9, 12, 16–19 of table 5). The strong mixing of states in the even-parity complex with $J = 1/2$ ($2s_{1/2}2s_{1/2}(0)1s_{1/2} + 2p_{1/2}2p_{1/2}(0)1s_{1/2} + 2p_{3/2}2p_{3/2}(0)1s_{1/2}$) leads to non-zero values of the radiative rates A_r (column 3) for the $E212-P232$ and $E212-P234$ transitions (line 1 and 3 from the bottom of table 5). The largest value of $Q_d(j, i)$ corresponds to the largest value of the effective emission rate coefficient $C_S^{\text{eff}}(j, i)$ when the ratio of E_S to kT_e is not very large.

For illustration of application of generated atomic data, we have constructed the synthetic spectra of Li-like ions that might be measured in future tokamak experiments. In particular, figures 3 and 4 show examples of synthetic dielectronic satellite spectra for Li-like Mo and W ions

Table 6. Energies (E in eV), radiative rates (A_r in s^{-1}), autoionization rates (A_a in s^{-1}) and intensity factors (Q_d in s^{-1}) for the $1s2l2l'-1s^22l''$ transitions in Li-like praseodymium, $Z = 59$. $A[B]$ means $A \times 10^B$. Experimental values from [30] are given for comparison.

jj designations	E	A_r	$\sum A_r$	A_a	Q_d	E [30]
$2p_{1/2}2p_{3/2}(1)1s\ 1/2$	$2p_{1/2}$	37 478.3	6.99[11]	6.91[15]	3.12[13]	6.29[09]
$2p_{3/2}2p_{3/2}(2)1s\ 3/2$	$2p_{1/2}$	37 446.3	2.35[10]	1.37[16]	4.55[13]	3.11[08]
$2s_{1/2}2p_{3/2}(2)1s\ 3/2$	$2s_{1/2}$	36 950.9	1.51[15]	1.51[15]	1.08[14]	4.02[14]
$2p_{1/2}2p_{3/2}(1)1s\ 1/2$	$2p_{3/2}$	36 930.6	6.91[15]	6.91[15]	3.12[13]	6.22[13]
$2s_{1/2}2p_{3/2}(1)1s\ 1/2$	$2s_{1/2}$	36 918.1	8.68[15]	8.68[15]	4.92[13]	9.78[13]
$2p_{3/2}2p_{3/2}(2)1s\ 3/2$	$2p_{3/2}$	36 898.7	1.37[16]	1.37[16]	4.55[13]	1.82[14]
$2s_{1/2}2p_{3/2}(1)1s\ 3/2$	$2s_{1/2}$	36 877.3	8.10[15]	8.10[15]	7.67[13]	3.04[14]
$2p_{1/2}2p_{3/2}(2)1s\ 3/2$	$2p_{1/2}$	36 874.6	8.62[15]	1.08[16]	1.30[14]	4.10[14]
$2p_{3/2}2p_{3/2}(0)1s\ 1/2$	$2p_{1/2}$	36 856.1	9.54[15]	1.41[16]	5.48[11]	7.42[11]
$2p_{3/2}2p_{3/2}(2)1s\ 5/2$	$2p_{3/2}$	36 851.3	2.53[15]	2.53[15]	1.06[14]	6.11[14]
$2p_{1/2}2p_{3/2}(1)1s\ 3/2$	$2p_{1/2}$	36 825.9	2.78[14]	2.60[15]	8.50[12]	3.63[12]
$2s_{1/2}2p_{1/2}(1)1s\ 1/2$	$2s_{1/2}$	36 371.4	3.53[15]	3.53[15]	1.64[14]	3.13[14]
$2p_{1/2}2p_{3/2}(2)1s\ 3/2$	$2p_{3/2}$	36 327.0	2.19[15]	1.08[16]	1.30[14]	1.04[14]
$2p_{3/2}2p_{3/2}(0)1s\ 1/2$	$2p_{3/2}$	36 308.5	4.54[15]	1.41[16]	5.48[11]	3.53[11]
$2p_{1/2}2p_{1/2}(0)1s\ 1/2$	$2p_{1/2}$	36 297.3	6.23[15]	6.23[15]	5.11[12]	1.02[13]
$2p_{1/2}2p_{3/2}(2)1s\ 5/2$	$2p_{3/2}$	36 285.6	4.48[15]	4.48[15]	6.01[13]	3.56[14]
$2p_{1/2}2p_{3/2}(1)1s\ 3/2$	$2p_{3/2}$	36 278.2	2.32[15]	2.60[15]	8.50[12]	3.03[13]
$2s_{1/2}2p_{1/2}(1)1s\ 3/2$	$2s_{1/2}$	36 273.6	4.11[15]	4.11[15]	1.40[13]	5.58[13]
$2s_{1/2}2p_{1/2}(0)1s\ 1/2$	$2s_{1/2}$	36 261.4	4.11[15]	4.11[15]	1.80[12]	3.59[12]
$2s_{1/2}2s_{1/2}(0)1s\ 1/2$	$2p_{1/2}$	36 087.1	2.93[14]	3.08[14]	1.91[14]	2.24[14]
$2p_{1/2}2p_{1/2}(0)1s\ 1/2$	$2p_{3/2}$	35 749.7	1.59[12]	6.23[15]	5.11[12]	2.60[09]
$2s_{1/2}2s_{1/2}(0)1s\ 1/2$	$2p_{3/2}$	35 539.4	1.52[13]	3.08[14]	1.91[14]	1.16[13]

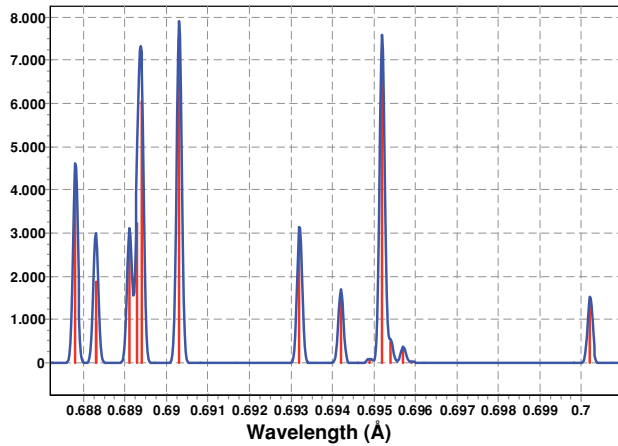


Figure 3. Synthetic spectra (red) of dielectronic satellite lines ($1s2l2l'-1s^22l''$) from the Mo^{39+} ion at $T_e = 7.5$ keV for $\lambda = 0.687-0.701$ Å. A resolving power, $R = \lambda/\Delta\lambda = 5000$, is assumed to produce a Gaussian profile (blue). The scale in the ordinate is in units of $10^{-13} \text{ cm}^3 \text{ s}^{-1}$.

produced by the $1s2l2l'-1s^22l''$ transitions. The effective emission rate coefficients $C_S^{\text{eff}}(j, i)$ and Gaussian profiles with spectral resolution $R \equiv \lambda/\Delta\lambda = 5000-3000$ are used to synthesize these spectra (see [17] for details). In particular, Li-like spectra cover the spectral ranges from 0.687 to 0.701 Å for Mo and from 0.204 to 0.212 Å for W. The most prominent dielectronic satellite lines are due to $1s2p^2D_{5/2}-1s^22p^2P_{3/2}$, $1s2p^2D_{3/2}-1s^22p^2P_{1/2}$ and $1s2s2p^2P_{1/2,3/2}-1s^22s^2S_{1/2}$ transitions.

The details of investigation of the possible use of spectral lines from highly ionized tungsten (W) ions to measure transport and other physical properties of ITER plasmas were

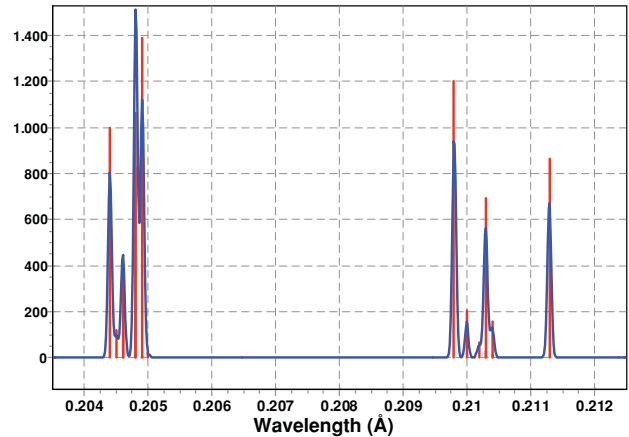


Figure 4. Synthetic spectra (red) of dielectronic satellite lines ($1s2l2l'-1s^22l''$) from the W^{71+} ion at $T_e = 40$ keV for $\lambda = 0.204-0.212$ Å. A resolving power, $R = \lambda/\Delta\lambda = 3000$ is assumed to produce a Gaussian profile (blue). The scale in the ordinate is in units of $10^{-13} \text{ cm}^3 \text{ s}^{-1}$.

recently published by Feldman *et al* [53] and are not subject of this paper.

4. Results and comparison with other theory and experiment

We calculated wavelengths, radiative rates, autoionization rates, Auger energies, branching ratios, intensity factors and effective emission rate coefficients for the $1s2l2l'-1s^22l''$ transitions in lithium-like ions within the framework of RMBPT. The radiative rates were obtained in both length and velocity forms, which are seen to be identical. Comparisons of our RMBPT energies with available experimental data for

Table 7. Auger energies (E_S in keV) and autoionization rates (A_a in s^{-1}) for the $1s2l2l'$ states in Li-like mercury, $Z = 80$. Comparison with measurements from [32]. $A[B]$ means $A \times 10^B$.

jj designations	E_S	A_a	E_S [32]
$2p_{1/2}2p_{3/2}(1)1s\ 1/2$	51.193	2.33[13]	
$2p_{3/2}2p_{3/2}(2)1s\ 3/2$	51.160	3.51[13]	
$2p_{3/2}2p_{3/2}(2)1s\ 5/2$	51.087	1.02[14]	51.064(6)
$2p_{1/2}2p_{3/2}(2)1s\ 3/2$	48.932	1.38[14]	48.918(9)
$2p_{3/2}2p_{3/2}(0)1s\ 1/2$	48.898	1.59[12]	
$2p_{1/2}2p_{3/2}(1)1s\ 3/2$	48.881	9.06[12]	
$2p_{1/2}2p_{3/2}(2)1s\ 5/2$	48.857	4.55[13]	
$2p_{1/2}2p_{1/2}(0)1s\ 1/2$	46.707	5.86[12]	
$2s_{1/2}2s_{1/2}(0)1s\ 1/2$	46.389	2.73[14]	46.358(4)
$2s_{1/2}2p_{3/2}(2)1s\ 3/2$	48.869	1.10[14]	48.845(5)
$2s_{1/2}2p_{3/2}(1)1s\ 1/2$	48.787	4.36[13]	
$2s_{1/2}2p_{3/2}(1)1s\ 3/2$	48.727	9.19[13]	48.844(6)
$2s_{1/2}2p_{1/2}(1)1s\ 1/2$	46.635	3.09[14]	46.611(6)
$2s_{1/2}2p_{1/2}(0)1s\ 1/2$	46.459	1.87[12]	
$2s_{1/2}2p_{1/2}(1)1s\ 3/2$	46.447	1.59[13]	

high- Z ions are shown in tables 6–8. RMBPT values of wavelengths and radiative rates are compared with MCDF calculations in table 9. We illustrate our theoretical results for intensity factors as a function of nuclear charge Z in figure 5. The cusps seen in some of the curves are discussed below.

Energies (E in eV), radiative rates A_r , autoionization rates A_a and relative intensity factors Q_d for the $1s2l2l' - 1s^22l''$ transitions in Li-like praseodymium, $Z = 59$, are listed in table 6. In this table, we compare our RMBPT transition energies with the two measured energies given in [30]. The relative intensity factors Q_d for these transitions are equal to 2.66 and 1.68 in units of $10^{14} s^{-1}$. It should be noted that there are at least six other transitions with $Q_d > 10^{14} s^{-1}$.

Auger energies E_S and autoionization rates A_a for the $1s2l2l'$ states in Li-like mercury, $Z = 80$, are presented

in table 7. Our RMBPT values of Auger energies E_S are compared with measured ones for the strongest DR resonances [32]. Of the 15 possible $1s2l2l'$ states, 6 correspond to observed DR resonances. The differences between our RMBPT values and experimental data are about 14–30 eV (0.03–0.06%), except for the $2s_{1/2}2p_{3/2}(1)1s\ 3/2$ level where the difference is about 0.24%. It should be noted that we use jj designations as did A J González Martínez *et al* [32]. However, our coupling scheme ($2s_{1/2}2p_j(J_{12})1s\ J$) is different from the one used in [32] ($1s2s_{1/2}(J_{12}2p_j)J$). Nevertheless, final results obtained with the same basis set should be independent of the coupling scheme. We note that the levels ‘He₃’ and ‘He₅’ in table 1 of [32] have identical jj -coupling designations. Our designations shown in the first column of table 7 are different. This must be a misprint in [32]. The third column of table 7 lists the values of autoionization rates A_a . The 6 identified resonances [32] have the largest A_a values among the 15 values included in table 7.

In table 8, we compare our RMBPT values of the energies E for the $2p_{3/2} - 2s$ transitions in Li-like uranium ($Z = 92$), thorium ($Z = 90$) and tungsten ($Z = 74$) ions with experimental measurements obtained by Beiersdorfer *et al* [54, 55]. We include the RMBPT results for Be- and B-like ions ($Z = 92, 90, 74$) from Safronova *et al* [35, 36] in table 8. The $2s2p_{3/2}(1) - 2s2s(0)$ and $2s2p_{1/2}2p_{3/2}(J) - 2s^22p_{1/2}$ transitions are considered. One can see from table 8 that the difference between RMBPT and experimental values for Li-like ions (0.02–0.03%) is larger than for Be-like ions (0.002–0.017%) and for B-like ions (0.006–0.012%). There are two reasons for this difference. We treat here the $1s2l2l'$ states as three-electron states and use Dirac basis set of functions; the $1s^22s_{1/2}$ and $1s^22p_{3/2}$ states are treated in the same way. The $2s2p_{3/2}(1)$, $2s2s(0)$ states in Be-like ions and $2s2p_{1/2}2p_{3/2}(J)$, $2s^22p_{1/2}$ states in B-like ions were evaluated with Dirac–Fock

Table 8. Energies (E in eV) of the $2s - 2p_{3/2}$ transitions in Li-, Be- and B-like uranium ($Z = 92$), thorium ($Z = 90$) and tungsten ($Z = 74$) ions, respectively. RMBPT values are compared with measurements given in [54, 55]. The RMBPT values for Be-like and B-like ions are from [35, 36].

Key	jj designations	Ion	RMBPT	Exp [54]	Ion	RMBPT	Exp [55]	Ion	RMBPT	
Li	$2p_{3/2}$	2s	U ⁸⁹⁺	4457.81	4459.37 ± 0.25	Th ⁸⁷⁺	4024.35	4025.23 ± 0.14	W ⁷¹⁺	1695.42
Be	$2s2p_{3/2}(1)$	2s2s(0)	U ⁸⁸⁺	4501.602	4501.72 ± 0.07	Th ⁸⁶⁺	4068.360	4068.47 ± 0.13	W ⁷⁰⁺	1741.371
B1	$2s2p_{1/2}2p_{3/2}(3/2)$	2s ² 2p _{1/2}	U ⁸⁷⁺	4520.838	4521.39 ± 0.60	Th ⁸⁵⁺	4089.629	4089.92 ± 0.50	W ⁶⁹⁺	1768.960
B2	$2s2p_{1/2}2p_{3/2}(1/2)$	2s ² 2p _{1/2}	U ⁸⁷⁺	4521.121	4521.39 ± 0.60	Th ⁸⁵⁺	4089.473	4089.92 ± 0.50	W ⁶⁹⁺	1766.900

Table 9. Wavelengths (λ in Å) and radiative rates (A_r in s^{-1}) for the $1s2s2p - 1s^22s$ transitions in Li-like Fe²³⁺ and Mo³⁹⁺. Designations: $E = 2s^2(^1S)1s$, $C = 2s2p(^1P)1s$, $K = 2s2p(^3P)1s$, $F = 2p^2(^1S)1s$, $F = 2p^2(^1D)1s$, $M = 2p^2(^3P)1s$, $S = 1s^22s$, and $P = 1s^22p$. The digits after a capital letter mean $(2S + 1)(2L + 1)(2J + 1)$. The RMBPT and MZ results are compared with the MCDF results given in [18, 19]. $A[B]$ means $A \times 10^B$.

LS labels	Wavelengths (λ in Å)			Radiative rates (A_r in s^{-1})			Wavelengths (λ in Å)			Radiative rates (A_r in s^{-1})		
	RMBPT	MZ	[18]	RMBPT	MZ	[18]	RMBPT	MZ	[19]	RMBPT	MZ	[19]
Li-like molybdenum, $Z = 42$						Li-like iron, $Z = 26$						
$C234 - S212$	0.687 76	0.687 63	0.6878	1.85[14]	1.88[14]	1.61[14]	1.8564	1.8563	1.8564	6.36[11]	7.78[11]	1.33[12]
$C232 - S212$	0.688 26	0.688 12	0.6883	2.08[15]	2.32[15]	2.09[15]	1.8572	1.8571	1.8572	1.72[14]	1.79[14]	1.76[14]
$K234 - S212$	0.689 25	0.689 12	0.6893	2.63[15]	2.94[15]	2.63[15]	1.8611	1.8610	1.8612	4.71[14]	4.87[14]	4.68[14]
$K232 - S212$	0.693 20	0.692 73	0.6932	1.20[15]	1.30[15]	1.17[15]	1.8637	1.8635	1.8638	3.10[14]	3.19[14]	3.04[14]
$K434 - S212$	0.695 44	0.695 03	0.6955	6.67[14]	6.92[14]	6.92[14]	1.8739	1.8738	1.8740	1.44[13]	1.59[13]	1.67[13]
$K432 - S212$	0.695 93	0.695 52	0.6960	1.98[14]	2.03[14]	2.05[14]	1.8749	1.8748	1.8751	4.53[12]	4.92[12]	5.17[12]

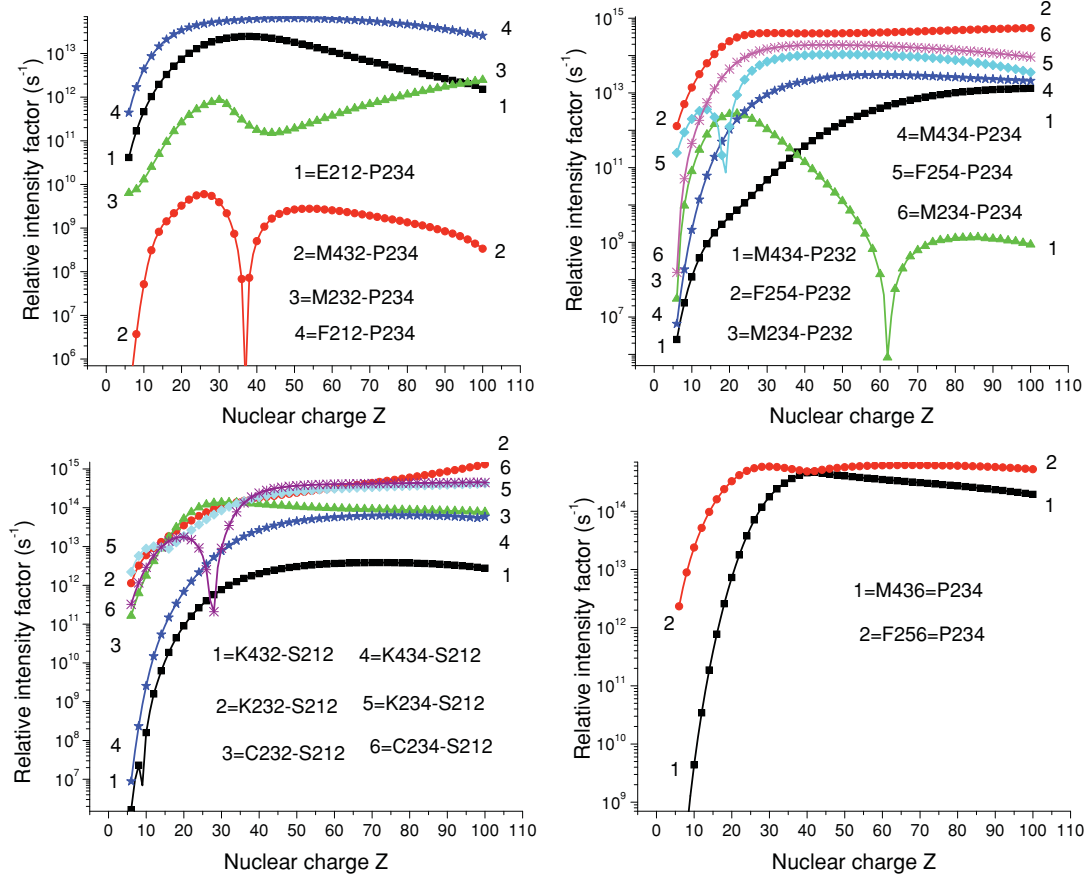


Figure 5. Relative intensity factor Q_d for the $1s2l2l' - 1s^22l''$ transitions as a function of nuclear charge Z . Designations: $E = 2s^2(^1S)1s$, $C = 2s2p(^1P)1s$, $K = 2s2p(^3P)1s$, $F = 2p^2(^1S)1s$, $F = 2p^2(^1D)1s$, $M = 2p^2(^3P)1s$, $S = 1s^22s$, and $P = 1s^22p$. Digits after the capital letters (i.e. $K432$) denote $(2S+1)(2L+1)(2J+1)$.

wavefunction with including $1s^2$ as a core. The second cause of the differences is the treatment of the QED contribution. It was shown in [35] that E_{Lamb} in U^{88+} ion for the $2s2p_{3/2}(1) - 2s2s(0)$ transition is equal to 37.887 eV contributing 0.84% to the total transition energy shown in table 8. We mentioned previously that we treat the QED contribution for a many-electron system as a sum of one-electron contributions and include screening. There are more elaborate methods to evaluate the QED contribution for a many-electron ion (see, for example, [37]), but making use of such methods here would take us well beyond the scope of the present work. We estimate the accuracy of our phenomenological treatment of QED to be about 10% of the sum of one-electron QED contributions. That gives us 3.8 eV or 0.08% in the case of the $2s2p_{3/2}(1) - 2s2s(0)$ transition in Be-like uranium.

Wavelengths and radiative rates A_r for the $1s2s2p - 1s^22s$ transitions in Li-like Fe^{23+} and Mo^{39+} are listed in table 9. We use the designations previously used in table 5: $C = 2s2p(^1P)1s$, $K = 2s2p(^3P)1s$ and $S = 1s^22s$. Our RMBPT results are compared with the results obtained with the MZ code. We already mentioned that the RMBPT code is the relativistic version of the MZ code since both include the second-order contributions to the correlation corrections. Our RMBPT and MZ results are compared in table 9 with

very recent results presented in [18, 19] where a relativistic multi-configuration Dirac-Fock (MCDF) technique was used for computing the transition wavelengths and rates. We find excellent agreement between all three codes for the wavelengths (0.02–0.07%) but not for radiative transition rates A_r . The smallest differences between the three codes for the A_r values are found for the $K434 - S212$ and $K432 - S212$ transitions (0–3.7%) in the case of $Z = 42$ and for the $C232 - S212$, $K234 - S212$ and $K4232 - S212$ transitions (0.6–4.7%) in the case of $Z = 26$. The RMBPT and MCDF results for the $C234 - S212$ transition in the case of $Z = 26$ differ by a factor of 2.

Relative intensity factors Q_d for the $1s2l2l' - 1s^22l''$ transitions as a function of nuclear charge Z are shown in four panels of figure 5. For high- Z ions, we find that Z dependence becomes almost constant for most transitions. With increasing Z the values of radiative rates A_r become larger than the values of autoionization rates A_a , since $A_r \sim Z^4$ for dipole-allowed transitions, while A_a changes only slightly with Z . As a result, Q_d becomes proportional to A_a (see equation (3)). We observe reciprocal ratios of radiative and autoionization rates (A_r and A_a) for low- Z ions; the values of A_r become smaller than those of A_a . In this case, the relative intensity factor Q_d becomes proportional to A_r (equation (3)). Cusps in the A_r curves

occur whenever the corresponding matrix element, which is a smooth function of Z , changes sign. For example, such cusps occur for the $F254-P234$ and $C234-S212$ transitions (curve 5 of the top right panel and curve 6 of the bottom left panel in figure 5 near $Z = 19$ and $Z = 28$, respectively).

5. Conclusion

In the present paper, we calculated a set of atomic data related to the dielectronic recombination of He-like ions into Li-like ions, obtained by means of the second-order RMBPT method. The resulting atomic data, which included energy levels, wavelengths, radiative transition probabilities and autoionization rates were used to synthesize dielectronic satellite spectra.

Our reduced matrix elements included correlation corrections from Coulomb and Breit interactions. Both length and velocity forms of the matrix elements were evaluated to verify the complete agreement between the two results. Second-order RMBPT transition energies were used in our evaluation of transition rates. The non-radiative matrix elements were calculated in the first-order RMBPT. Although the RMBPT data were calculated for the broad range of nuclear charges Z from 6 to 100, the main emphasis as well as a detailed discussion of correlation contributions to the evaluated characteristics was made for lithium-like tungsten, $Z = 74$.

Synthetic spectra of dielectronic satellite lines ($1s2l2l' - 1s^22l''$) of the Mo^{39+} ($T_e = 7.5$ keV) and W^{71+} ($T_e = 40$ keV) ions are constructed using the complete set of RMBPT data. These results are relevant to spectroscopic diagnostics of plasmas of a broad range of parameters, including very high temperature plasmas such as those expected in the future ITER device.

Acknowledgments

This research was sponsored by the US Department of Energy under the OFES grant DE-FG02-08ER54951 and in part under the NNSA Cooperative agreement DE-FC52-06NA27588.

References

- [1] Skinner Charles H 2009 *Phys. Scr. T* **134** 014022
- [2] Biedermann C, Radtke R, Seidel R and Pütterich T 2009 *Phys. Scr. T* **134** 014026
- [3] Reader J 2009 *Phys. Scr.* **134** 014023
- [4] Loch S D, Pindzola M S, Ballance C P, Griffin D C, Whiteford A D and Pütterich T 2006 *AIP Proc.* **874** 233
- [5] Gabriel A N 1972 *Mon. Not. R. Astron. Soc.* **160** 99
- [6] Safronova U I and Kharitonova V N 1969 *Opt. Spectra* **27** 300
- [7] Bhalla C P, Gabriel A N and Presnyakov L P 1975 *Mon. Not. R. Astron. Soc.* **172** 359
- [8] Vainshtein L A and Safronova U 1978a *At. Data Nucl. Data Tables* **21** 49
- [9] Bely-Dubau F, Gabriel A N and Volonté S 1979 *Mon. Not. R. Astron. Soc.* **186** 405
- [10] Vainshtein L A and Safronova U 1980 *At. Data Nucl. Data Tables* **25** 311
- [11] Faucher P and Dubau J 1985 *Phys. Rev. A* **31** 3672
- [12] Chen M H 1986 *At. Data Nucl. Data Tables* **34** 301
- [13] Nilsen J 1988 *At. Data Nucl. Data Tables* **38** 339
- [14] Safronova U, Safronova M S, Bruch R and Vainshtein L A 1995 *Phys. Scripta* **51** 471
- [15] Shevelko V P and Vainshtein L A 1995 *Atomic Physics for Hot Plasmas* (Ristol: Pergamon Press)
- [16] Kato T, Safronova U I, Shlyaptseva A, Cornille M, Dubau J and Nilsen J 1997 *At. Data Nucl. Data Tables* **67** 225
- [17] Safronova U, Vasilyev A and Smith R K 2000 *Can. J. Phys.* **78** 1055
- [18] Hao LiangHuan, Jiang Gang, Song Shuqiang and Hu Feng 2008 *At. Data Nucl. Data Tables* **94** 739
- [19] Hou HaiJun, Jiang Gang, Hu Feng and Hao LiangHuan 2009 *At. Data Nucl. Data Tables* **95** 125
- [20] Bernshtam V A, Zarnitsky Yu, Ralchenko Yu, Vainshtein L A, Weingarten L and Maron Y 2009 *Phys. Scr.* **79** 035303
- [21] Boiko V P, Pikuz S A, Safronova U I and Faenov A Y 1978a *Mon. Not. R. Astron. Soc.* **185** 789
- [22] Boiko V P, Faenov A Y and Pikuz S A 1978b *J. Quant. Spectrosc. Radiat. Transfer* **19** 11
- [23] Group TFR, Dubau J and Loulergue M L 1981 *J. Phys. B: At. Mol. Phys.* **15** 1007
- [24] Bitter M *et al* 1985 *Phys. Rev. A* **32** 3011
- [25] Bombarda F, Giannella R, Kallne G J T E, Bely-Dubau F, Faucher P, Cornille M, Dubau J and Gabriel A N 1988 *Phys. Rev. A* **37** 504
- [26] Beiersdorfer P, Chen M H, Mars R E, Shneider M B and Walling R S 1991 *Phys. Rev. A* **44** 396
- [27] Beiersdorfer P, Phillips T, Jacobs V L, Hill K W, Bitter M, von Goeler S and Kahn S M 1993a *ApJ* **409** 846
- [28] Tarbutt M R, Barnsley R, Peacock N J and Silver J D 2001 *J. Phys. B: At. Mol. Opt. Phys.* **34** 3977
- [29] Skinner C H 2008 *Can. J. Phys.* **86** 285
- [30] Thorn D B, Brown G V, Clementson J H, Chen H, Chen M, Beiersdorfer P, Boyce K R, Kilbourne C A, Porter F S and Kelley R L 2008 *Can. J. Phys.* **86** 241
- [31] González Martínez A J *et al* 2005 *Phys. Rev. Lett.* **94** 203201
- [32] González Martínez A J *et al* 2006 *Phys. Rev. A* **73** 052710
- [33] Nakamura Nobuyuki, Kavanagh Anthony P, Watanabe Hirofumi, Sakaue Hiroyuki A, Li Yueming, Kato Daiji, Currell Fred J and Ohtani Shunsuke 2008 *Phys. Rev. Lett.* **073203**
- [34] Safronova U I and Safronova M S 2004 *Can. J. Phys.* **82** 743
- [35] Safronova M S, Johnson W R and Safronova U I 1996a *Phys. Rev. A* **53** 4036
- [36] Safronova M S, Johnson W R and Safronova U I 1996b *Phys. Rev. A* **54** 2850
- [37] Blundell S A, Johnson W R, Safronova M S and Safronova U I 2008 *Phys. Rev. A* **77** 032507
- [38] Mohr P J 1974a *Ann. Phys., NY* **88** 26
- [39] Mohr P J 1974b *Ann. Phys., NY* **88** 52
- [40] Mohr P J 1975 *Phys. Rev. Lett.* **34** 1050
- [41] Safronova U I and Shestakov A F 1983 *Relativistic and Radiative Effects in Atoms and Ions* (Moscow: Scientific Council on Spectroscopy, USSR Academy of Science) pp 58–88
- [42] Blundell S A 1993 *Phys. Rev. A* **47** 1790
- [43] Yerokhin V A, Indelicato P and Shabaev V M 2006 *Phys. Rev. Lett.* **97** 253004
- [44] Kim Y-K, Baik D H, Indelicato P and Desclaux J P 1991 *Phys. Rev. A* **44** 148
- [45] Safronova U I, Johnson W R and Livingston A E 1999 *Phys. Rev. A* **60** 996

- [46] Johnson W R, Plante D R and Sapirstein J 1995 *Adv. At. Mol. Opt. Phys.* **35** 255
- [47] Safronova U I 1989 *Phys. Scr. T* **26** 59
- [48] Brage T, Fischer Ch Froese and Vaeck N 1993 *J. Phys. B: At. Mol. Opt. Phys.* **26** 621
- Q1** [49] Cowan R D and Wilson M 1991 *J. Phys. B: At. Mol. Opt. Phys.* **24** 111
- [50] Drake G W F 2006 *Handbook of Atomic, Molecular, and Atomic Physics* (Berlin: Springer)
- [51] Vainshtein L A and Safronova U I 1978b *At. Data Nucl. Data Tables* **21** 49
- [52] Dubau J and Volonté S 1980 *Rep. Prog. Phys.* **43** 199
- [53] Feldman U, Seely J F, Landi E and Ralchenko Yu 2008 *Nucl. Fusion* **48** 045004
- [54] Beiersdorfer P, Knapp D, Marrs R E, Elliott S R and Chen M H 1993b *Phys. Rev. Lett.* **71** 3939
- [55] Beiersdorfer P, Osterheld A, Elliott S R, Chen M H, Knapp D and Reed K 1995 *Phys. Rev. A* **52** 2693

Queries

- (1) Author: Please check whether the year is okay as set in reference [49].
- (2) Author: Please be aware that the colour figures in this article will only appear in colour in the Web version. If you require colour in the printed journal and have not previously arranged it, please contact the Production Editor now. Else amend the reference to color in the captions to figures [3](#) and [4](#).

Reference linking to the original articles

References with a volume and page number in blue have a clickable link to the original article created from data deposited by its publisher at CrossRef. Any anomalously unlinked references should be checked for accuracy. Pale purple is used for links to e-prints at arXiv.